Daily Global Land Parameters Derived from AMSR-E and AMSR2 (Version 3.1)

Contact Information:
Jinyang Du, and John S. Kimball
Numerical Terradynamic Simulation Group (NTSG)
The University of Montana
Missoula MT, 59812

Email:
jinyang.du@ntsg.umt.edu; johnk@ntsg.umt.edu

URL:
http://files.ntsg.umt.edu/data/LPDR_v3/GeoTif

Document last updated: 04/05/2023

Table of Contents

I. Data introduction

The Version 3 global land parameter data record (LPDR) was generated using calibrated microwave brightness temperature (T_b) records from the Advanced Microwave Scanning Radiometer for EOS (AMSR-E) on the NASA EOS Aqua satellite, and the Advanced Microwave Scanning Radiometer 2 (AMSR2) sensor on the JAXA GCOM-W1 satellite. The latest LPDR release (Version 3.1) includes an additional data year (2021), but with no other changes from the Version 3 algorithms or product format; the resulting data record extends from from Jun. 19, 2002 to Dec. 31, 2021.

Primary LPDR inputs include JAXA AMSR2 L1R orbital swath T_b retrievals, calibrated against similar RSS (Remote Sensing Systems) Version 7 AMSR-E T_b records, where individual T_b frequencies and ascending and decending orbit retrievals are calibrated separately (Du et al. 2014). The daily multi-frequency, ascending and decending orbit, and vertically and horizontally polarized T_b records are used as primary inputs to an iterative retrieval algorithm for simultaneous estimation of a set of higher order land parameters (Du et al. 2017; Du et al. 2018). The resulting land parameter record includes 30-day temporally smoothed fractional open water cover *(fw)* and daily (non-smoothed) fractional open water *(fwns)* estimates*;* daily surface air temperature minima and maxima (T_{mn} and T_{mx}, ~2 m height); X-band (10.7 GHz) vegetation optical depth (*VOD*); surface (10.7 GHz) volumetric soil moisture (*vsm*); atmosphere total collumn precipitable water vapor (*PWV*); and surface atmospheric Vapor Pressure Deficit (*VPD,* ~2 m height). The resulting LPDR is available in a 25-km resolution global EASE-Grid (v1) projection. The global retrievals are affected by land cover conditions within the sensor footprint used for generating the 25 km gridded resolution T_b record; the land parameter estimates were only carried out over land for classified non-precipitating, snow and ice-free conditions. Accordingly, ancillary quality control (QC) bit flag files were also generated recording the average land coverage within each 25 km grid cell and indicating other quality factors, including non-retrieval conditions for missing T_b observations, frozen surface, snow cover, active rainfall, and identified radio frequency interference (RFI) in the 10.7, and 18.7 GHz channels. A daily QC frozen flag is included that distinguishes the predominant freeze-thaw (FT) condition of the land surface within each 25-km grid cell as derived from a daily FT classification of

AMSR 36.5 GHz T_b retrievals from a global FT Earth System Data Record (FT-ESDR, Kim et al. 2016); here the FT-ESDR defined QC flag is used to distinguish non-frozen conditions as a pre-requisite for higher-order LPDR retrievals.

The LPDR Version 3 (v3) data are aimed to provide an enhanced data record over prior (v1, v2) LPDR releases in terms of improved retrieval accuracy, addition of new land parameter retrievals, and longer period-of-record. The LPDR v3 record provides consistent land parameter retrievals spanning both AMSR-E and AMSR2 (AMSR-E/2) operational records, that are suitable for science quality evaluations of key land parameters important to ecosystem processes.

II. LPDR changes from prior versions

The LPDR v3 data record effectively replaces prior LPDR releases. The LPDR v3 record shares the same algorithms with previous product versions except that a new *VPD* land parameter is included, which is calculated from the LPDR daily surface temperature and atmosphere precipitable water vapor retrievals. The v3 record extends the AMSR (AMSR-E and AMSR2) global land parameter observations over a longer period of record (2002-2021), enabled from continuing AMSR2 operations. The v3 record also reflects numerous algorithm refinements and performance enhancements benefitting from ongoing calibration, validation and science application studies. A detailed description of the LPDR v3 algorithms and changes are provided elsewhere (Du et al. 2017; Du et al., 2018), while major v3 refinements and updates from prior (v1, v2) LPDR releases are summarized below and in Section III:

- The LPDR is derived from calibrated T_b retrieval records from both AMSR-E and AMSR2, allowing continuity of the data record, which extends from Jun. 19, 2002 to Dec. 31, 2021; the latest release (v3.1) includes three additional years beyond the earlier v2.0 release, which ended Dec. 31, 2018.
- The *PWV* algorithm is refined by additional accounting of cloud liquid water and surface terrain effects; and improved by calibrating against similar retrievals from the Atmospheric Infrared Sounder (AIRX2RET Version 6).
- A refined estimation of T_{mx} and T_{mn} that considers terrain and latitude effects;
- Addition of a daily surface (~2m height) atmospheric vapor pressure deficit (*VPD*, kPa) land parameter derived from the AMSR LPDR surface temperature and *PWV* retrievals (see Du et al., 2018 for details);
- An improved X-band (10.7 GHz) *vsm* retrieval using a weighted averaging strategy and dynamic selection of vegetation scattering albedo effects (Du et al. 2016).
- Updated FT frozen QC flag derived from the AMSR 36.5 GHz T_b based FT classification record, which is part of the latest (v5) FT-ESDR global product. Note that different from previous versions which set frozen QC flag if frozen conditions were detected from both morning and afternoon FT retreivals, the frozen flag was set for a given date and pixel where frozen condition was detected from either afternoon or morning AMSR obervations.

- Corrections were made to an issue with the LPDR v3 data record, which was caused by incomplete reading of the Tb data record of 2016. The data record affected by the issue is for the data period from DOY 204 to 366 of year 2016 of the previous release (v3.0). The issue has been resolved in the latest release (v3.1) by re-processing the data for 2016.

III. Algorithm description

The Version 3 algorithm was derived based on the general framework of the original Version 1 iterative retrieval algorithm (Jones et al., 2010) and later algorithm revisions (Du et al., 2015, 2016, 2017, 2018).

The LPDR algorithms first derive effective surface temperature (*Ts*), T_{mx} and T_{mn}, *fw* and *PWV* using an iterative algorithm approach that incorporates H- and V-polarized 18.7 GHz and 23.8 GHz T_b data and several temperature insensitive microwave indices (Jones et al., 2010). The X-band (10.7 GHz) *VOD* is then obtained by inverting the land-water microwave emissivity slope index, and surface (~ 0-1 cm depth) *vsm* is acquired after correcting for X-band atmosphere, *fw* and vegetation effects (Jones et al., 2010). Different from other available AMSR algorithms, the methodology exploits satellite multi-frequency T_b observations for synergistically retrieving multiple inter-connected land parameters, and with minimal requirements for other external ancillary inputs beyond the AMSR T_b observations; the LPDR algorithms also specifically account for the impacts of land surface open water on the *PWV*, T_{mx} and T_{mn}, *VOD* and *vsm* retrievals within a grid cell (Jones et al., 2010; Du et al., 2017).

Compared with prior LPDR releases (v1.0, v2.0) the Version 3 algorithm refinements include: (a) an empirical calibration of the AMSR derived estimation for *PWV* based on similar observations from AIRS (Du et al., 2015); (b) T_b screening for frozen land surface conditions identified using an existing global daily freeze-thaw (FT) data record (FT-ESDR) derived from a refined FT classification of 36.5 GHz T_b retrievals from the AMSR sensors (Kim et al., 2017); (c) improved AMSR estimations of T_{mn} and T_{mx} that consider terrain and latitude effects (Du et al., 2015); (d) refined AMSR X-band (10.7 GHz) *vsm* retrievals using a weighted averaging strategy and dynamic selection of vegetation scattering albedo effects (Du et al., 2016) and (e) an empirical *fw* calibration made for improving the *vsm* inversion (Du et al., 2017). To account for the differences between RSS V7 and V6 AMSR-E T_b retrievals which were separately used in Version 2 and Version 1 algorithms, values of the following empirical parameters including reference dry soil emissivities, reference pure water emissivities, and delta parameter for descending orbits were adjusted from the original values in (Jones et al., 2010). Accordingly, regressions were re-made for estimating *PWV*, T_{mn} and T_{mx} based on pre-defined procedures as detailed in (Du et al., 2017). For producing a consistent LPDR spanning the AMSR-E to AMSR2 observation periods, AMSR2 T_b data were empirically inter-calibrated against AMSR-E based on similar overlapping FY3B MWRI satellite sensor observations (Du et al., 2014). The gridded AMSR T_b data were calculated from overlapping sensor footprints using an Inverse

Distance Weighting interpolation method.

A new *VPD* parameter was included in the latest LPDR v3 release, in addition to the surface parameters included in earlier LPDR releases (v1.0, v2.0). The *VPD* (kPa) calculation relies on the determination of the saturation vapor pressure e_s (kPa) at a given air temperature T_a (°C) and the actual vapor pressure e_a (kPa). The dependence of e_s on T_a is theoretically described by the Clausius-Clapeyron relationship and normally approximated by the Magnus formula in applications. Similarly, e_a was calculated as the saturation vapor pressure at dew-point temperature Td (°C). Accordingly, the AMSR *VPD* was empirically estimated using *VPD* observations from global weather station observations and AMSR LPDR outputs related to surface air temperature and humidity. Specifically, the AMSR *VPD* record was derived using empirical regressions between the in situ *VPD* observations from weather stations and the corresponding AMSR LPDR parameters for surface temperature, vegetation transmissivity, *PWV*, *fw*, and ancillary inputs for surface elevation (*H*; km) and geographic latitude (*Lat*; radian). A detailed description of the VPD retrieval method and resulting LPDR VPD accuracy and global performance is given in (Du et al., 2018).

IV. Data File Information

The LPDR data files are provided in GeoTIFF (.tif) format. Each daily file contains a 3-D array (7 bands×1383 columns × 586 rows) of 32-bit float-type data containing all of the retrieved land parameters. The data are projected into 25 km global EASE-Grid (v1) format. The fill value is -999.0. Detailed data band information is described below:

Table 1. LPDR data band description

Band name	Parameter	Descriptions	Unit	Valid range
Band 1	*fw*	30-day smoothed open water fraction	dimensionless	0-1
Band 2	*fwns*	Non-smoothed open water fraction	dimensionless	0-1
Band 3	T_{mn} *or* T_{mx}	Daily surface air temperature minima or maxima, corresponding to descending or ascending pass retrievals	Kelvin	240- 340
Band 4	*PWV*	Vertically integrated atmospheric water vapor	mm	0-80
Band 5	*VOD*	Vegetation optical depth at 10.7 GHz	Neper	0-3
Band 6	*vsm*	Volumetric soil moisture at 10.7 GHz	cm^3/cm^3	0-1
Band 7	*VPD*	near-surface atmospheric Vapor Pressure Deficit	KPa	≥0

Additional bit-wise data quality files (QA) are provided in GeoTIFF (.tif) format for describing the quality information of LPDR data files. Each QA file corresponding to a LPDR data file contains a 2-D array (1383 columns × 586 rows) of 8-bit byte-type data. The data are projected into the same 25 km global EASE-Grid (v1) format. The fill value is 255. Detailed quality (QC) bit flag descriptions are listed below:

Table 2. LPDR data quality flag descriptions

Bit number	Land surface condition	Indication
1st	Frozen ground (FT-ESDR)	No LPDR retrieval
2nd	Snow or ice presence	No LPDR retrieval
3rd	Strong precipitation	No LPDR retrieval
4th	RFI at 18.7 GHz	No LPDR retrieval
5th	RFI at 10.65 GHz	No LPDR retrieval
6th	Dense vegetation with *VOD* > 2.3	Larger retrieval uncertainty
7th	Large water bodies with *fw* > 0.2	Larger retrieval uncertainty
8th	Saturated microwave signals with V-pol and H-pol Tb difference at 18 GHz or 23 GHz less than 1.0 K	Larger retrieval uncertainty

V. File naming convention

LPDR data file

AMSRU_Mland_{year}{day of year}{overpass (A or D)}.tif

The string "AMSRU_Mland" represents global land parameters derived from both AMSR-E and AMSR2 observations. The year string contains four digits. The day-of-year is the day in three digits since January 1 of the year. The overpass character is either 'A' for ascending (afternoon; P.M.) or 'D' for descending (morning; A.M.). The file extension "tif" is associated with the GeoTIFF file type.

QA file

AMSRU_Mland_{year}{day of year}{overpass (A or D)}_QA.tif

The QA files share the same naming convention with the LPDR data files except an additional descriptor "_QA" is added.

VI. LPDR accuracy and performance

A detailed LPDR (v3) accuracy and performance assessment was conducted over the global domain and is summarized elsewhere (Du et al. 2017; Du et al., 2018). A summary of LPDR performance for the primary land parameters is provided below.

Fractional open water

The AMSR-E (year 2010) and AMSR2 (year 2015) *fw* summer composites were compared with a finer spatial resolution static water map derived from MODIS-SRTM (MOD44W) observations. Both AMSR-E and AMSR2 results (Fig.1a, 1b) captured a similar global inundation pattern as MOD44W (Fig.1c) including major river systems such as the Amazon River and Yangtze River, and widespread inundation occurring within the pan-Arctic region.

Quantitative comparisons of LPDR *fw* summer means over the globe for years 2003 to 2010 and representing the AMSR-E full-year observation record and AMSR2 observations from 2013-2015 in relation to MOD44W are summarized in Table 3. The

resulting LPDR *fw* summer averages show overall favorable spatial correspondence with the MOD44W *fw* map ($R \geq 0.75$ and $RMSE \leq 0.06$). The AMSR2 portion of the LPDR shows an overall higher performance than AMSR-E, which may result from improved AMSR2 sensor footprint resolution relative to AMSR-E, enabling better land surface delineation.

Table 3. Comparisons of fw global averages over AMSR-E (2003-2010) and AMSR2 (2013-2015) periods in relation to the MOD44W static open water map. All products were projected into a consistent 25.0 km resolution EASE-GRID format; positive and negative bias indicates fw over- and under- estimation, respectively, relative to the static water map

AMSR-E/2 *fw* vs MOD44W						
	R*		RMSD*		Bias	
	Asc*	Dsc*	Asc*	Dsc*	Asc*	Dsc*
AMSR-E	0.77	0.75	0.06	0.06	0.02	0.01
AMSR2	0.79	0.78	0.05	0.05	0.02	0.01

* R denotes Pearson correlation coefficient; RMSD denotes Root Mean Square Difference; Asc and Dsc denote respective ascending and descending orbits.

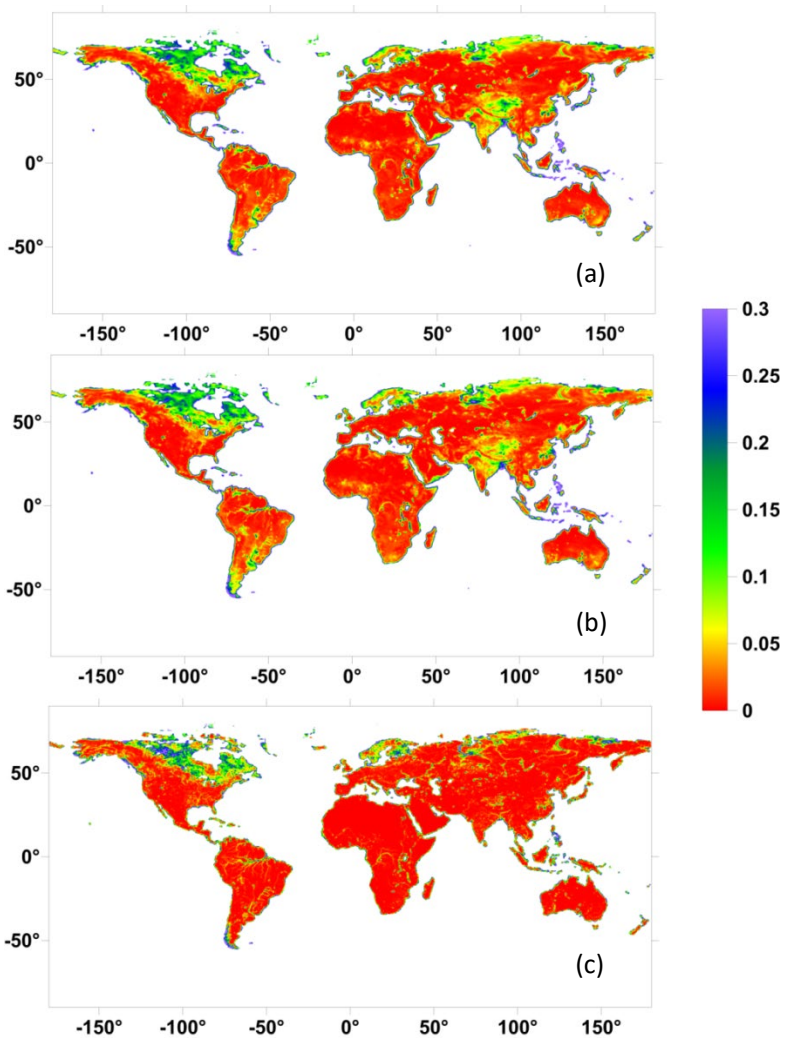

Fig.1 Summer composite (JJA) of 25-km global fractional water over land retrieved from AMSR-E ascending observations for year 2010 (a); AMSR2 ascending observations for year 2015 (b); and 25-km MOD44W static water map aggregated from original 250-m resolution (c).

Total precipitable water vapor and daily maximum/minimum air temperature

The resulting spatial distributions of *PWV* (Fig. 2) and T_{mx} (Fig. 3) summer composites were generated for AMSR-E (year 2010) and AMSR2 (year 2015) based on their daily ascending orbit retrievals. Similar to the previous results (Du et al., 2014), the *PWV* retrievals show a latitudinal gradient with higher values at lower latitudes and warmer regions consistent with the near-exponential relationship between atmospheric temperature and moisture holding capacity, except for dry desert regions distinguished by characteristicly lower *PWV* levels. The T_{mx} distributions also follow a similar latitudinal gradient as *PWV* but with more complex spatial variations affected by regional climate, land cover conditions and elevation gradients (Du et al., 2015).

The LPDR *PWV* and air temperature retrievals were quantitatively validated against NASA Aqua AIRS observations and in-situ temperature measurements at 142 global WMO weather station locations for selected years 2010 and 2013 (Table 4). The AMSR retrievals show strong agreement with the AIRS *PWV* product (R ≥ 0.91; RMSE ≤ 4.98 mm), though a slight *PWV* over estimation and under estimation is indicated for respective AMSR-E (bias ≤ 0.23 mm) and AMSR2 (bias ≥ -0.27 mm) portions of record (Table 4). The LPDR corresponded favorably with the WMO air temperature measurements (R ≥ 0.89; RMSE ≤ 3.46 ºC). The AMSR-E (2010) and AMSR2 (2013) retrievals show similar T_{mn} and T_{mx} retrieval accuracy, with associated RMSE differences within 0.13 K in relation to the WMO daily temperature measurements. However, the calibrated AMSR2 T_b record is not identical to that of AMSR-E as reflected by a maximum 0.40 ºC difference in their T_{mx} and T_{mn} retrieval biases against WMO measurements (Table 4).

Table 4. LPDR daily T_{mx}, T_{mn} and ascending/descending orbit based *PWV* accuracy in relation to respective in-situ air temperature measurements and AIRS *PWV* observations for 142 global WMO site locations for selected years 2010 (AMSR-E) and 2013 (AMSR2).

	T_{mx} (ºC)			T_{mn} (ºC)		
	R	RMSE	Bias*	R	RMSE	Bias
AMSR-E	0.92	3.42	0.60	0.89	3.32	0.02
AMSR2	0.92	3.46	0.20	0.89	3.19	0.21
	PWV (mm) from Ascending Orbits			*PWV* (mm) from Descending Orbits		
	R	RMSE	Bias	R	RMSE	Bias
AMSR-E	0.92	4.24	0.23	0.92	4.76	0.18
AMSR2	0.91	4.57	-0.27	0.91	4.98	-0.20

*Bias is calculated from retrievals minus observations.

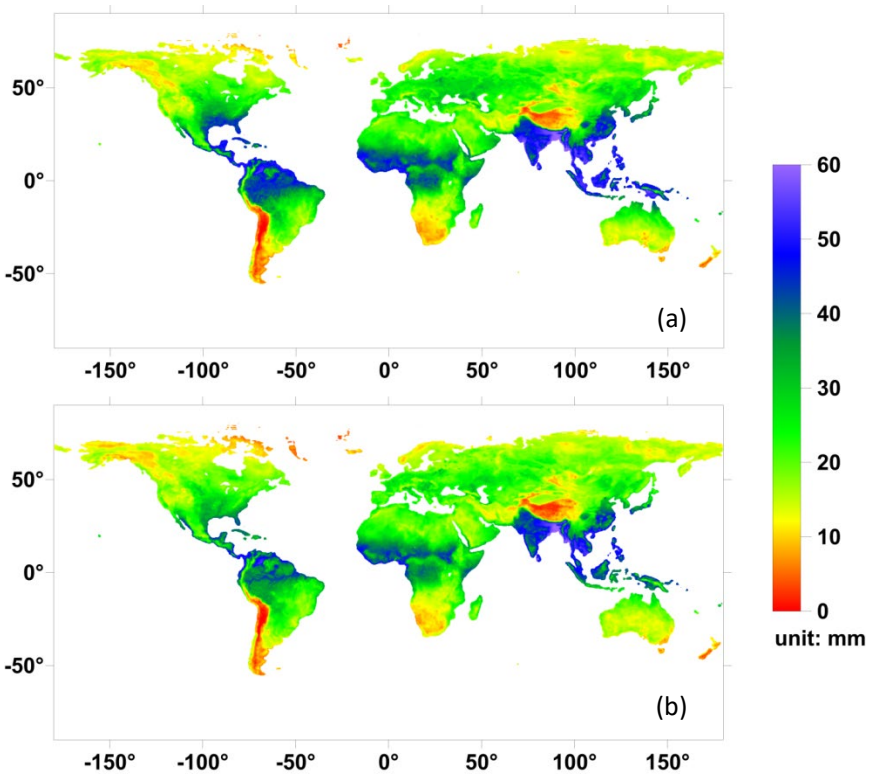

Fig.2 Summer composite (JJA) of 25-km precipitable water vapor (*PWV*, mm) over land retrieved from AMSR-E ascending observations for year 2010 (a); AMSR2 ascending observations for year 2015 (b).

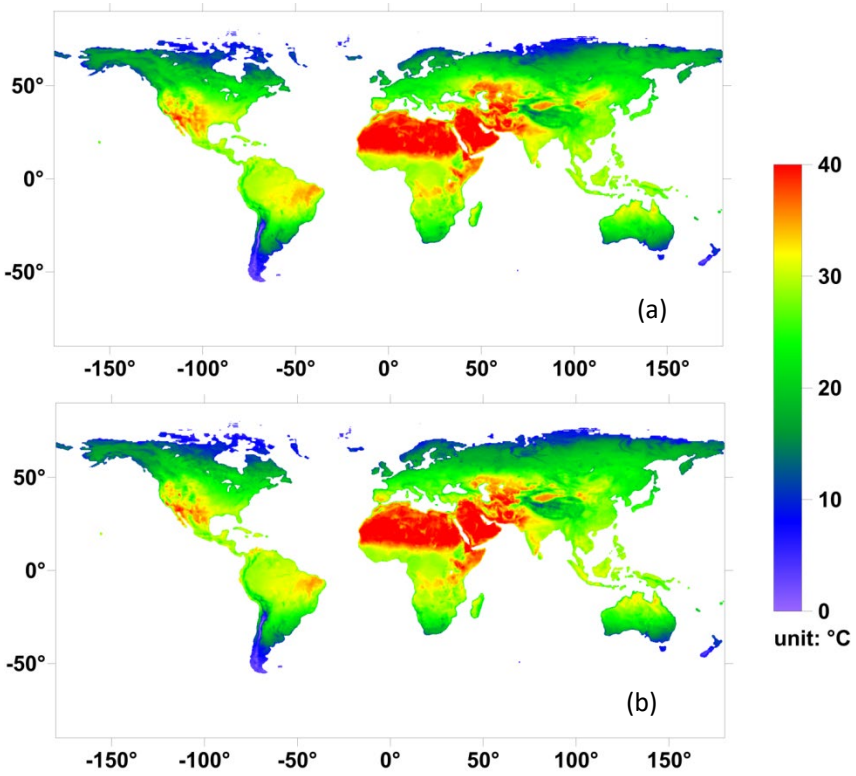

Fig.3 Summer composite (JJA) of 25-km global maximum daily surface air temperature (T_{mx}) over land retrieved from AMSR-E ascending observations for year 2010 (a); AMSR2 ascending observations for year 2015 (b).

Vegetation optical depth

The resulting spatial distributions of X-band (10.7 GHz) *VOD* Northern-Hemisphere summer composites (JJA) were generated for AMSR-E (year 2010) and AMSR2 (year 2015) based on their daily ascending orbit retrievals. Both AMSR-E and AMSR2 *VOD* retrievals from the LPDR show a similar global distribution pattern (Fig.4). Highest *VOD* values are found in wet tropical rainforest regions including the Amazon Basin, Congo Basin and Southeast Asia, and high-latitude boreal forest regions; while the lowest *VOD* values are shown in desert or barren land areas such as the Sahara Desert, Taklamakan Desert, Sonoran desert and Central Australia. Moderate *VOD* values generally reflect median vegetation conditions of the regions including the grassland in the Central US, the Africa ecoclimatic transition zone Sahel and major rice fields in Central China and India. However, caution is needed when analyzing long-term *VOD* changes especially for higher biomass regions where AMSR T_b observations and *VOD* retrievals tend to get saturated and become more sensitive to the sensor inter-calibration accuracy (Du et al., 2017).

The LPDR derived *VOD* (10.7 GHz) was compared with the GIMMS3g NDVI climatology monthly means for the aggregate 2003-2010 and 2013 to 2015 observation record. Here, the mean seasonal cycle in *VOD* and NDVI is depicted for major IGBP global land cover types, including evergreen needleleaf forest (ENF), evergreen broadleaf forest (EBF), deciduous needleleaf forest (DNF), deciduous broadleaf forest (DBF), grassland

and cropland. Both *VOD* and NDVI display similar seasonal cycles represented by their mean monthly time series (R ≥ 0.88) (Table 5). Differences in NDVI correspondence between the ascending and descending orbit *VOD* records may reflect regional *VOD* retrieval uncertainties contributed by deficiencies in the underlying LPDR algorithm assumptions and parameterizations, which are discussed in (Du et al., 2017).

Table 5. Pearson correlations [R] between LPDR *VOD* (10.7 GHz) and GIMMS3g NDVI climatology monthly means for the aggregate 2003-2010 and 2013 to 2015 observation record. The comparisons were made for all global vegetation and selected land cover areas, including: ENF, EBF, DNF, DBF, grassland and cropland. Both products were projected into a consistent 25.0 km resolution EASE-GRID format. *VOD* results are delineated for LPDR ascending and descending orbit records**.**

Pearson correlation coefficient	Global	ENF	EBF	DNF	DBF	Grassland	Cropland
Ascending	0.88	0.71	0.22	0.89	0.20	0.90	0.67
Descending	0.94	0.90	-0.12	0.94	0.87	0.95	0.84

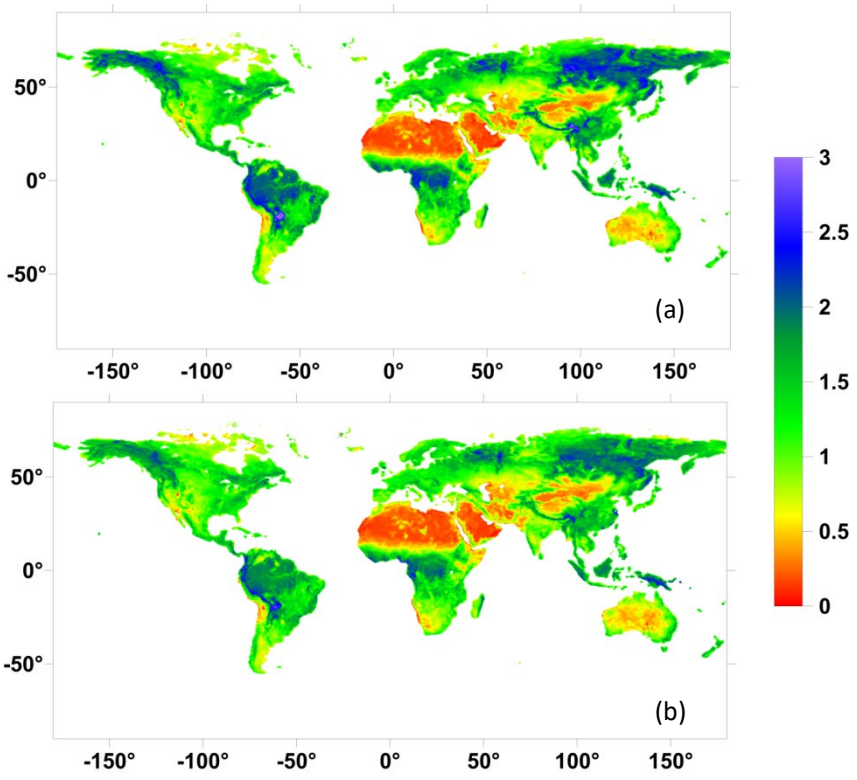

Fig.4 Summer composite (JJA) of 25-km global *VOD* (10.7 GHz) retrieved from AMSR-E ascending observations for year 2010 (a); AMSR2 ascending observations for year 2015 (b).

Soil Moisture

The AMSR soil moisture retrievals were compared against globally distributed validation watershed measurements as shown in Table 6. The overall retrieval accuracy is similar to that presented in (Du et al., 2016) with a general better performance of descending (AM) orbit retrievals than the ascending (PM) orbit observations. The global

soil moisture distributions (Fig.5) derived from both AMSR-E and AMSR2 are similar to each other and consistent with the known global climatology including characteristically wet surface soil moisture conditions in northern high latitude areas, drier soil moisture extremes in deserts and semi-arid regions, such as the African Sahara desert, Southern California Desert, and central and western desert regions of Australia. Here, the AMSR vsm sensitivity and performance reflects surface (0-2 cm depth) soil conditions captured by the 10.7 GHz T_b retrievals; whereas, T_b sensitivity to soil conditions and associated *vsm* performance is expected to be degraded in more densely vegetated (VOD) areas.

Table 6: Summary of satellite LPDR soil moisture retrieval accuracy in relation to in situ surface soil moisture measurements from four globally distributed validation watersheds.

Statistics	Little River (USA; 2003-2005)	Little Washita (USA;2003-2005)	Naqu (China; 2010-2011)	Yanco (Australia; 2009-2011)	All Sites*
Ascending Orbits					
R	0.63	0.76	0.79	0.76	0.82
RMSE*	0.04	0.04	0.05	0.06	0.05
Bias	0.04	0.05	-0.10	-0.04	0.01
Descending Orbits					
R	0.70	0.73	0.83	0.79	0.84
RMSE*	0.03	0.04	0.04	0.06	0.04
Bias	0.07	0.09	-0.06	-0.03	0.04

R is coefficient coefficient; RMSE (Root Mean Square Error) and Bias are in cm^3/cm^3. *RMSE and All Sites statistics except bias are calculated with watershed bias corrected.

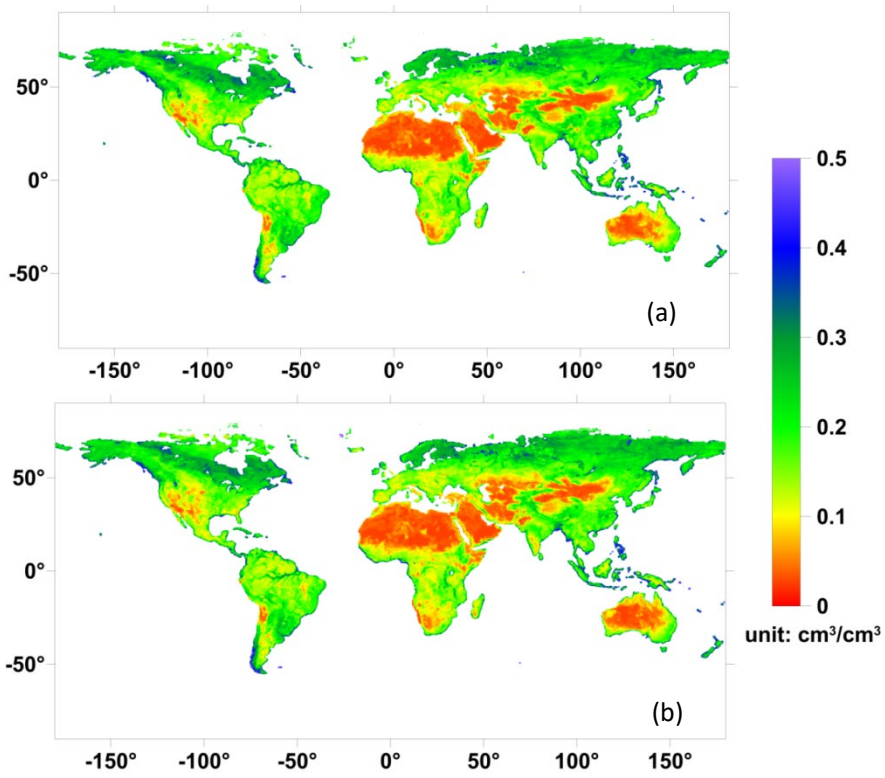

Fig.5 Summer composite (JJA) of 25-km X-band (10.7 GHz) global volumetric soil moisture (*vsm*) retrieved from AMSR-E ascending observations for year 2010 (a); AMSR2 ascending observations for year 2015 (b).

Near-surface Atmospheric Vapor Pressure Deficit

The AMSR-derived *VPD* record (Fig.6) shows strong correspondence (correlation coefficient ≥ 0.80, p-value < 0.001) and overall good performance (0.48 kPa $\leq$ RMSE $\leq$ 0.69 kPa) against independent observations from global weather stations and global reanalysis (GMAO MERRA-2) data. The estimated AMSR *VPD* retrieval uncertainties vary with land cover type, satellite observation time, and underlying LPDR data quality (Du et al. 2018).

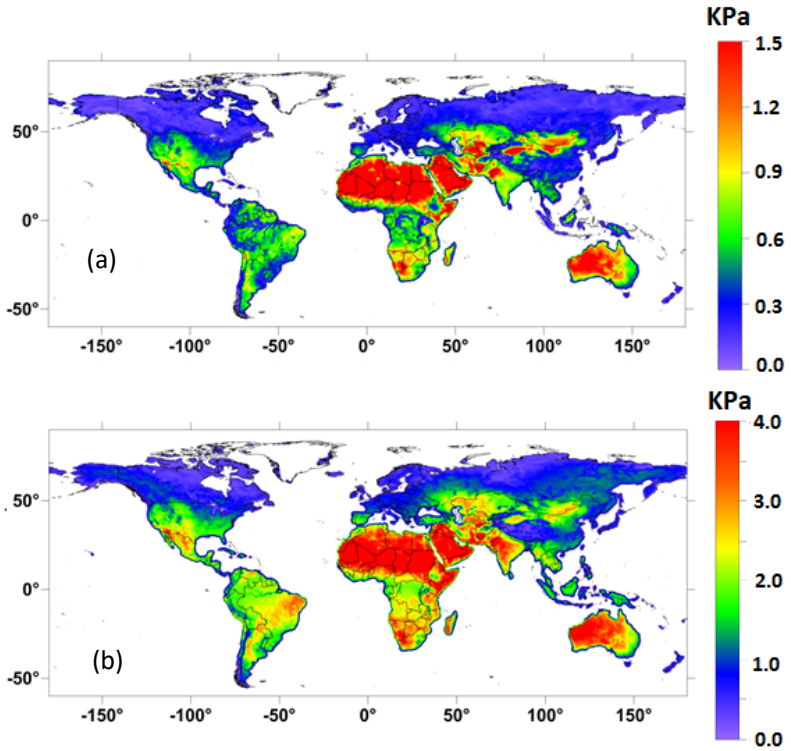

Fig.6 Mean annual *VPD* at 1:30 AM (a) and 1:30 PM (b) local time derived from AMSR over 2010 .

VII. Data version

Version 1: Original data released on 1/21/2010 followed by grid and flag updates on 9/12/2011 and data processed through the end of the AMSR-E record on 4/23/2012. The v1 algorithms and product performance are described in the literature (Jones et al, 2010).

Version 2.0: Data released on 3/22/2017. Data were processed for the entire AMSR-E operational record (06/19/2002 to 10/04/2011) and part of the AMSR2 record (07/24/2012 to 12/31/2018). The associated v2 algorithms were revised from the prior v1 algorithm (Jones et al, 2010) as detailed in the literature (Du et al., 2014, 2015 and 2016) and summarized in (Du et al., 2017).

Version 3: Initial data release on 3/22/2021, and updated on 04/05/2023 (v3.1). Data were processed for the entire AMSR-E operational record (06/19/2002 to 10/04/2011) and part of the AMSR2 record (07/24/2012 to 12/31/2021), with planned updates and LPDR continuity enabled from continuing AMSR2 operations. The associated v3 algorithms are the same as the prior v2.0 algorithm (Du et al., 2017) except for minor algorithm and product refinements, and the addition of a new *VPD* land parameter, following (Du et al., 2018).

VIII. Data citation, acknowledgements and references

As a condition of using these data, you must cite the use of this data set using the following citation. For more information, see our Use and Copyright Web page:

Du, J., and J. S. Kimball. 2022. *Daily Global Land Surface Parameters Derived from AMSR-E and AMSR2, Version 3*. [Indicate subset used]. Boulder, Colorado USA. NASA National Snow and Ice Data Center Distributed Active Archive Center. doi: http://dx.doi.org/10.5067/JIKQZ6WO5C5M. [Date Accessed].

As a condition of using these data, we request that you acknowledge the author(s) of this data set by referencing the following peer-reviewed publication:

Du, J., J.S. Kimball, L.A. Jones, Y. Kim, J. Glassy, and J.D. Watts, 2017. A global satellite environmental data record derived from AMSR-E and AMSR2 microwave earth observations, 2017. *Earth System Science Data*, 9, 791-808, https://doi.org/10.5194/essd-9-791-2017.

Acknowledgements: These data were generated through a grant from the NASA MEaSUREs (Making Earth System Data Records for Use in Research Environments) program (80NSSC18K0980). This work was conducted at the University of Montana under contract to NASA.

Other References are listed below:

[1] Du, J., Kimball, J.S., Reichle, R.H., Jones, L.A., Watts, J.D. and Kim, Y.: Global satellite retrievals of the near-surface atmospheric vapor pressure deficit from AMSR-E and AMSR2. *Remote sensing*, 10(8), p.1175,2018.

[2] Kim, Y., Kimball, J. S., Glassy, J., and Du, J.: An Extended Global Earth System Data Record on Daily Landscape Freeze-Thaw Status Determined from Satellite Passive Microwave Remote Sensing, *Earth Syst. Sci. Data*., 9 (1), 133-147, 2017.

[3] Du, J.; Kimball, J.S.; Jones, L. A . Passive Microwave Remote Sensing of Soil Moisture Based on Dynamic Vegetation Scattering Properties for AMSR-E. *IEEE Transactions on Geoscience and Remote Sensing.* 2016, 54 (1), 597-608.

[4] Du, J., J.S. Kimball, and L.A. Jones. Satellite microwave retrieval of total precipitable water vapor and surface air temperature over land from AMSR2. *IEEE Transactions on Geoscience and Remote Sensing,* 2015, 53 (5), 2520-2531 (DOI 10.1109/TGRS.2014.2361344).

[5] Du, J.; Kimball, J.S.; Shi, J.; Jones, L.A.; Wu, S.; Sun, R.; Yang, H. Inter-Calibration of Satellite Passive Microwave Land Observations from AMSR-E and AMSR2 Using Overlapping FY3B-MWRI Sensor Measurements. *Remote Sens.* 2014, *6*, 8594-8616.

[6] Jones, L.A.; Ferguson, C.R.; Kimball, J.S.; Zhang, K.; Chan, S.T.K.; McDonald, K.C.; Njoku, E.;Wood, E. Satellite microwave remote sensing of daily land surface air temperature minima and maxima from AMSR-E. *IEEE J. Sel. Top. Appl. Earth Obs. Remote Sens*. 2010, 3, 111–123.